Journal of Catalysis **191,** 105–115 (2000)
doi:10.1006/jcat.1999.2777, available online at http://www.idealibrary.com on IDEAL®

Quantification of the Primary Processes in Aqueous Heterogeneous Photocatalysis Using Single-Stage Oxidation Reactions

Lev Davydov and Panagiotis G. Smirniotis[1]

Department of Chemical Engineering, University of Cincinnati, Cincinnati, Ohio 45221-0171

Received August 10, 1999; revised December 6, 1999; accepted December 7, 1999

The present study aimed at the quantification of primary photocatalytic processes occurring over irradiated semiconductors. The photodegradation of HCOOH was selected as a probe reaction since it follows a single-stage oxidation mechanism (yielding CO_2 and H_2O), thus not relying on the formation of stable intermediate products or multiple reactions. This reaction was used to determine lumped kinetic parameters of UV-assisted photocatalysis in semiconductor slurries. A modified Fricke dosimeter ($Fe^{2+} \rightarrow Fe^{3+}$) was utilized to determine the exact concentrations of reactive oxygen species in the slurry, such as $^{\bullet}OH$, $HO_2^{\bullet}$, $^{\bullet}O_2^-$, and H_2O_2. These experiments yielded maxima in the concentrations of these species during the first few minutes of reaction with the subsequent attainment of a steady state. The rate of generation of reactive oxygen species characterizes the true oxidative power of photocatalysts, and it was found to increase with the catalyst concentration and reach a plateau value in the vicinity of 0.25 g/l of catalyst. This generation rate follows the pattern Ishihara ST21 ≈ Hombikat UV100 ≈ Degussa P25 > Aldrich anatase; its value for Aldrich anatase is approximately one-third of that for the other catalysts. The effect of direct oxidation by valence-band holes was studied using the oxidation of NO_2^- to NO_3^- and proved to be minimal. From the kinetic data of the photodegradation of formic acid, rates of primary photocatalytic processes, such as radical generation (R_{gen}) and electron–hole recombination (R_{rec}), were determined with our methodology. In particular, R_{rec} was found to be inversely proportional to the BET surface area of the catalyst following the sequence Aldrich anatase > Degussa P25 > Ishihara ST21 ≈ Hombikat UV100. Using the present methodology, the quantum yield of a particular photocatalyst can be predicted satisfactorily from its radical generation rate. It should be noted that such quantum yield depends on the catalyst concentration and reactor setup to a much lesser extent than the traditionally used quantum yield for phenol photodegradation, since the latter process is accompanied by multiple secondary oxidation reactions. Thus, the method proposed provides a convenient procedure for a thorough study on semiconductor photocatalysis and can serve as a common means of photocatalyst characterization.

Key Words: **single stage oxidation; TiO_2; primary radicals; Fricke dosimetry; photocatalysis; formic acid.**

INTRODUCTION

Reactive oxygen species (1) play a crucial role in heterogeneous photocatalysis aimed at the degradation of organic compounds. They are formed on the surface of the photocatalyst and react with either adsorbed or dissolved organic species. Turchi and Ollis (2) showed that the major reaction route of photocatalytic oxidation involves the hydroxyl radical attack. Several researchers proposed a number of methods to quantify hydroxyl radical formation. α-Abstraction of hydrogen from methanol was proposed as a probe reaction (3), which leads to a presumably stable intermediate (formaldehyde) according to the following reaction:

$$CH_3OH \xrightarrow[-H_2O]{+^{\bullet}OH,O_2} H_2CO \xrightarrow[-H_2O]{+^{\bullet}OH,O_2} HCOOH \xrightarrow[-H_2O]{+^{\bullet}OH,O_2} CO_2. \quad [1]$$

In this way it was possible to estimate reaction rates and quantum yields of hydroxyl radical production by titania in aqueous solutions. 3-Carboxyproxyl was also utilized as an $^{\bullet}OH$ trap (4), which forms a stable diamagnetic adduct. This allowed the estimation of the hydroxyl radicals' concentrations in irradiated semiconductor slurries.

The above methods for quantification of primary radicals production can adequately characterize the "oxidative power" of a particular photocatalyst. However, the main disadvantage of both methods is that they rely on the formation of an intermediate compound, which can further degrade, especially under high-intensity light conditions. For this reason, a single-stage oxidation reaction is highly desirable. There are suggestions in the literature (5) that the photocatalytic degradation of formic acid represents such a reaction (it produces CO_2 and H_2O directly). Other researchers investigated the photocatalytic and photoelectrocatalytic degradation of formic acid (the last stage of reaction [1]) in aqueous solution. For example, a ZnO photoelectrode was used for this reaction (6, 7). It was shown that the electron of the activated formate ion (formyloxy radical) is released to oxygen when the latter

[1] To whom correspondence should be addressed.

0021-9517/00 $35.00

is present in the system. This electron transfer happened in preference to the zinc oxide electrode as no significant increase in the anodic photocurrent took place. A study on the photodegradation of formic acid over a platinized CdS semiconductor (8) revealed that the lower pH is favorable for this reaction. Immobilized TiO_2 was also utilized to study the UV-assisted degradation of formic acid (9, 10). Benderskii *et al.* (11) investigated the photodegradation at high initial concentrations of formic acid.

Photochemical studies (12) and photoelectrocatalytic studies (6) suggest that the last step of the above reaction (degradation of formic acid in the presence of oxygen) is a single-stage oxidation reaction. Moreover, oxygen prevents the formyloxy radicals from dimerizing (12), making HCOOH an ideal candidate to study primary processes of photocatalysis. As a supplement, chemical dosimetry will be used in the present study as a means to quantify reactive oxygen species and primary photocatalytic processes (electron–hole recombination and reactive oxygen species formation) occurring in irradiated semiconductors. The dependence of each reaction rate on the average volumetric rate of radiant energy absorption as well as the BET surface area of the catalysts will be elucidated.

THEORY

The present analysis will be based on the primary reactions presented below, which describe completely all the chemical features of the phenomenon under consideration. On the basis of the similarity of certain reactions (namely, radical formation and recombination) they were lumped into one reaction.

- A quantum of radiation with energy higher than the band gap of the semiconductor ($\lambda < 385$ nm) impinges on a titania particle, producing an electron–hole pair:

$$TiO_2 \xrightarrow{h\nu} h^+ + e^- \qquad R_{ex} = \mu C_{cat} G. \qquad [2.1]$$

The rate of the above reaction is proportional to the photon absorption rate (assuming that the excitation is 100% efficient) as the concentration of the semiconductor in the slurry is constant throughout the reaction vessel.

- Some of the resulting electrons and holes recombine by the following reaction:

$$h^+ + e^- \rightarrow TiO_2 + \text{heat} \qquad R_{rec} = k_{rec}[h^+][e^-]. \quad [2.2]$$

The rate of recombination is dependent on both the number of holes and the number of electrons in the bulk of the semiconductor particle.

- Valence-band holes form primary radicals:

$$\begin{aligned} h^+ + OH^- &\rightarrow {}^\bullet OH \\ h^+ + H_2O &\rightarrow {}^\bullet OH + H^+ \qquad R_{h^+} = k_{h^+}[h^+]. \end{aligned} \qquad [2.3]$$

The concentration of ions and water in the aqueous solution is abundant. For this reason we assume the rate of surface reaction of holes to be proportional to the hole concentration on the surface of the semiconductor.

- Conduction-band electrons are scavenged by oxygen, forming multiple peroxide species by the following reactions:

$$\begin{aligned} e^- + O_2 &\rightarrow {}^\bullet O_2^- \\ H^+ + {}^\bullet O_2^- &\rightarrow {}^\bullet HO_2 \\ 2H^+ + {}^\bullet O_2^- + e^- &\rightarrow H_2O_2 \qquad R_{e^-} = k_{e^-}[e^-]. \end{aligned} \qquad [2.4]$$

It should be noted that the limiting step of the above reaction scheme is the surface reaction, assuming that all peroxide species are equally active. It was shown (1) that the limiting stage in radical formation is the electron transfer between the solid surface of titania and adsorbed molecular oxygen. Furthermore, the rate of this consecutive reaction [2.4] must be equal to the electron transfer rate. Since an excessive amount of oxygen is supplied to the reactor, the rate is proportional to the concentration of electrons.

- Some of the reactive oxygen species ${}^\bullet OH$, ${}^\bullet HO_2$, and H_2O_2 (denoted by O^∇) recombine with the surface of titania:

$$TiO_2 + O^\nabla \rightarrow TiO_2 + \tfrac{1}{2}O_2 \qquad R_{ct} = k_{ct}[O^\nabla]. \qquad [2.5]$$

The recombination of surface radicals is represented by electron transfer between the surface radical and the semiconductor surface. Furthermore, its rate is proportional only to the concentration of surface radicals formed. The two groups of radicals (produced by reactions [2.3] and [2.4]) can be lumped into one group when considering their recombination with the surface of titania. This is because their recombination takes place via electron transfer, and the rate of recombination must be equal for both groups of radicals in order to maintain the electrical neutrality of the particle.

- The remaining radicals engage in a chemical reaction with the organic species present in the system:

$$\begin{aligned} HCOO^- + O^\nabla &\rightarrow H_2O + CO_2 + e^- \\ R_s &= k_s[O^\nabla][HCOO^-]. \end{aligned} \qquad [2.6]$$

The rate of this reaction is proportional to both the concentration of surface radicals and the concentration of the reactant in the solution. Others (1, 2) proposed similar reactions for the description of the primary processes occurring in photocatalysis.

As a summary of the background knowledge about the oxidation of formic acid, the following assumptions are adopted in the present study when developing the kinetic model for the photodegradation of formic acid.

1. H_2O, O_2,and radicals produced are in the adsorbed state as the lifetime of radicals in the bulk solution is low (12).

2. Formic acid reacts with surface radicals, not with holes. The latter process may occur at relatively high (1 M) concentrations of HCOOH (11) when formic acid can compete with water for the catalytic sites of titania. This assumption will be justified experimentally below.

3. The electron produced in reaction [2.6] is scavenged by oxygen (6, 12).

4. The rates of photolysis and dark heterogeneous degradation of formic acid are negligible. They were found to be within the experimental error rendered by titration in the degradation of formic acid in the absence of catalyst and at a Degussa P25 concentration of 0.25 g/l, respectively.

5. Steady state is achieved with respect to holes, electrons, and reactive oxygen species.

The following derivations are conducted in order to develop the reaction rate law (based on known quantities) for the photodegradation of formic acid over irradiated semiconductors (titania). From the balance of electrons and holes at steady state one can deduce the following:

$$\mu C_{\text{cat}} G - k_{\text{rec}}[\text{h}^+][\text{e}^-] - k_{\text{h}^+}[\text{h}^+] = 0 \qquad [3.1.1]$$

$$\mu C_{\text{cat}} G - k_{\text{rec}}[\text{h}^+][\text{e}^-] - k_{\text{e}^-}[\text{e}^-] = 0. \qquad [3.1.2]$$

The above system yields $k_{\text{h}^+}[\text{h}^+] = k_{\text{e}^-}[\text{e}^-]$. Solving for the concentration of electrons and holes results in the following relations:

$$[\text{h}^+] = -\frac{k_{\text{e}^-}}{2k_{\text{rec}}} + \sqrt{\frac{k_{\text{e}^-}^2}{4k_{\text{rec}}^2} + \frac{k_{\text{e}^-}}{k_{\text{rec}}k_{\text{h}^+}}\mu C_{\text{cat}} G} \qquad [3.2.1]$$

$$[\text{e}^-] = -\frac{k_{\text{h}^+}}{2k_{\text{rec}}} + \sqrt{\frac{k_{\text{h}^+}^2}{4k_{\text{rec}}^2} + \frac{k_{\text{h}^+}}{k_{\text{rec}}k_{\text{e}^-}}\mu C_{\text{cat}} G}. \qquad [3.2.2]$$

The steady-state balance of reactive oxygen species can be derived from Eqs. [2.3]–[2.6] and it takes the form

$$k_{\text{h}^+}[\text{h}^+] + k_{\text{e}^-}[\text{e}^-] - k_{\text{ct}}[\text{O}^{\triangledown}] - k_{\text{s}}[\text{O}^{\triangledown}][\text{HCOO}^-] = 0. \qquad [3.3]$$

Solving the above equation leads to the steady-state concentration of these species:

$$[\text{O}^{\triangledown}] = \frac{k_{\text{h}^+}[\text{h}^+] + k_{\text{e}^-}[\text{e}^-]}{k_{\text{ct}} + k_{\text{s}}[\text{HCOO}^-]}. \qquad [3.4]$$

Hence, the local reaction rate of formic acid photodegradation by combining equations [2.6], [3.2.1], [3.2.2], and [3.4] becomes

$$R_{\text{HCOO}^-} = \frac{(k_{\text{s}}/k_{\text{ct}})[\text{HCOO}^-]}{1 + (k_{\text{s}}/k_{\text{ct}})[\text{HCOO}^-]} \frac{k_{\text{h}^+}k_{\text{e}^-}}{k_{\text{rec}}} \times \left[\sqrt{1 + 4\mu C_{\text{cat}} G \frac{k_{\text{rec}}}{k_{\text{h}^+}k_{\text{e}^-}}} - 1\right]. \qquad [3.5]$$

One can observe that the constant $(k_{\text{s}}/k_{\text{ct}})$ of the first term in the numerator represents the ratio of the photodegradation rate to the recombination of reactive oxygen radicals. The second multiplier represents the ratio of a product of radical generation rates to the electron–hole recombination rate. These two expressions of kinetic constants ($k_{\text{s}}/k_{\text{ct}}$ and $k_{\text{h}}k_{\text{e}}/k_{\text{rec}}$) can serve the purpose of photocatalyst characterization in their combined form as one can expect high photodegradation rates from photocatalysts with high values of both expressions. We will attempt, however, to obtain individual reaction rates of radical generation and electron–hole recombination. For this reason two experimental conditions may be considered. The first condition is that of a relatively high concentration of formic acid (greater than 5 mM, as will be proved experimentally), so that the unity in the denominator can be neglected. From such high-concentration experiments it will be possible to determine the parameter $k_{\text{h}^+}k_{\text{e}^-}/k_{\text{rec}}$ by plotting the reaction rate ($R^{(0)}$) as a function of the average square root of the absorbed photon flux.

In the second extreme case, the low concentration of the reactant (below 0.5 mM, as will be shown later) makes it possible to neglect the concentration term in the denominator, and the reaction becomes first order with respect to formic acid ($R^{(1)}$). Thus, for the same concentration of catalyst, light source, and other experimental conditions, two reaction rates can be determined:

$$R^{(0)} = \frac{k_{\text{h}^+}k_{\text{e}^-}}{k_{\text{rec}}} \left[\sqrt{1 + 4\mu C_{\text{cat}} G \frac{k_{\text{rec}}}{k_{\text{h}^+}k_{\text{e}^-}}} - 1\right] \qquad [3.6]$$

$$R^{(1)} = \frac{k_{\text{s}}}{k_{\text{ct}}}[\text{HCOO}^-]R^{(0)}. \qquad [3.7]$$

By observing the steady-state balance of radicals one can derive the total rate of radical generation in a particular photoreactor. This will allow a comparison of the performance of different photocatalysts on its basis. After these algebraic manipulations with the balance of electrons and holes (Eq. [3.1]) and active radicals (Eq. [3.3]) one arrives at the following relations:

$$R_{\text{gen}} = R_{\text{h}^+} + R_{\text{e}^-} = \frac{2 + (k_{\text{s}}/k_{\text{ct}})[\text{HCOO}^-]}{1 + (k_{\text{s}}/k_{\text{ct}})[\text{HCOO}^-]} R^{(0)} \qquad [3.8]$$

$$R_{\text{rec}} = \mu C_{\text{cat}} \bar{G} - \frac{2 + (k_{\text{s}}/k_{\text{ct}})[\text{HCOO}^-]}{1 + (k_{\text{s}}/k_{\text{ct}})[\text{HCOO}^-]} R^{(0)}. \qquad [3.9]$$

The quantum yield of any photochemical process is usually defined as the ratio of the rate of this process to the rate of energy absorption. If the absorption of radiation flux G_{a} brings about the rate of transformation R_n, the expression of the quantum yield can be written in the following fashion:

$$\Phi = \frac{R_n}{G_{\text{a}}}. \qquad [3.10]$$

Overall, the above methodology allows assessing the rates and quantum yields of primary photocatalytic processes,

such as active radical generation and electron–hole recombination, from simple experimental measurements. The knowledge of these rates will allow us to predict reaction rates and quantum yields in different photoreactors at different catalyst concentrations and create a common means of comparing different photocatalytic semiconductors.

EXPERIMENTAL

The experimental work performed in this study is aimed at testing the proposed methodology with selected photocatalysts. Two main categories of experiments were performed in the present study: high initial concentration of formic acid and low initial concentration of formic acid. Commercial titanias were evaluated for the photocatalytic degradation of formic acid. The titania powders utilized in the present study were Aldrich anatase (denoted as AA), Hombikat UV-100 (HK), Ishihara ST-21 (ST), and Degussa P25 (P25); their characteristics are shown in Table 1. As one can observe, these catalysts possess quite different optical and adsorption properties. The suspensions were prepared with the titania particles dispersed ultrasonically in aqueous solutions containing the appropriate amount of formic acid. Prior to each experiment, the UV lamp was warmed up for 5 min. Samples were withdrawn from the reactor and filtered on 0.2-μm membrane filters (Gelman Sciences) to remove the titania particles. The suspension temperature was maintained at $30 \pm 3^{\circ}$C. The concentration of the unreacted compound was measured by using a conductivity meter (VWR Scientific, golden cell, cell constant 10.25 cm^{-1}). It was calibrated by using standard solutions of formic acid with concentrations ranging from 0.001 to 20 mM. A quadratic curve passing through zero and the experimental points was fitted with an accuracy of 0.999; this curve was used for the conductivity–concentration correlation. The reaction mixtures were also tested for the presence of intermediates at differents times on stream by direct injection into a GC (HP 5890 Series II) equipped with a MS (HP-5972). No detectable amounts of intermediate compounds were found.

TABLE 1

Photocatalysts Employed in the Present Study

Catalyst	BET surface area,[a] m^2/g	Anatase content,[b] %	Primary particle size, nm	Extinction coefficient β,[c] L/(cm g)	Scattering albedo ω[c]
AA	10.0	99	100–200[d]	15.32	0.388
P25	75.0	70–80	~20[b]	23.50	0.663
HK	313.2	99	<10[b]	7.42	0.467
ST	64.0	95	~20[b]	9.32	0.562

[a] Measured with use of a Micromeritics Gemini 2320 surface analyzer at 77 K.

[b] According to the manufacturer's specifications.

[c] Measured spectrophotometrically with use of a Shimadzu 2501PC, equipped with a Shimadzu ISR 2200 integrating sphere.

[d] Determined by transmission electron microscopy (Siemens).

A modified Fricke dosimeter (13) was used to determine the overall concentration of reactive oxygen species in irradiated aqueous suspensions of titania. It consisted of 5 mM $FeSO_4$ (Fisher), 10 mM $CuSO_4$ (Fisher), and 20 mM H_2SO_4 (Fisher). During the reaction with reactive oxygen species Fe^{3+} ion is produced, and it was quantified by spectrophotometry (Shimadzu U160) at the wavelength of 304 nm. Standard quartz cuvettes with a path length of 1 cm were used. The absorbance by Fe^{3+} was correlated with the concentration of Fe^{2+} reacted and further used for calculations.

In the experiments on the photooxidation of nitrite ions, a 30 mM concentration of $NaNO_2$ (Fisher) was subjected to photolyses by different powders of titania under the same operating conditions. The unreacted nitrite was determined by titration using 0.005 mM $KMnO_4$ (Fisher) solution. The end point of titration was determined colorimetrically at the wavelength of 535 nm.

A conventional annular liquid-phase photocatalytic reactor (Ace Glass, Inc., Catalog No. 7868-10) was utilized for the study as described elsewhere (14). A glass stirring shaft assured mixing and circulation within the vessel. A double-walled quartz immersion well was placed in the middle of the reaction vessel. Its purpose was to allow the circulation of water for cooling the light source and the solution. The UV part of lamp radiation was also filtered by a Pyrex filter (7740, Ace Glass, Inc.) placed between the lamp and the immersion well. The thickness of the Pyrex filter was 2.38 mm, the inside diameter was 26 mm, and it allowed us to eliminate the far- and mid-UV bands ($\lambda < 320$ nm) of the emission spectrum of the lamp. The immersion-type UV radiation source was a 450-W (medium-pressure) mercury vapor quartz lamp (Ace Glass). Oxygen (Wright Brothers, 99.5%) was sparged into the solution at 500 cm^3/min through a fritted glass tube at the bottom of the vessel. With this flow rate no deposition on the walls of the reactor was observed. Such an oxygen flow rate did not lead to reactant stripping and entrainment into the gas phase.

The titania powders were also evaluated in a differential photoreactor (14) with the same lamp and cooling jacket but different thickness of the reaction zone. A conventional magnetic stirrer vigorously agitated the suspension in the reactor. A laboratory peristaltic pump (Masterflex 7017-21) was used to run the suspension through the reactor. An intermittent vessel was used for degassing of the suspension and for sample withdrawal. This vessel was also agitated by a magnetic stirrer in order to avoid sedimentation of titania and provide better dispersion of oxygen bubbles. Flexible plastic tubing connected the pump, vessel, and reactor. No reactant stripping was observed during the experiments.

A radiometer (International Light, Inc., Model IL 1700) was used to determine local incident photon flux densities

in the reactor. It was connected with a detector (International Light, Inc., Model SED033 #3435). A UV filter was employed in order to measure only the light of interest and its response exhibited a strong maximum at the wavelength of 355 nm. The incident radiation at R_I as well as the outgoing radiation at R_O was measured at various locations along the reactor length by the detector at the outer wall of the quartz cooling jacket.

A Shimadzu 2501PC spectrophotometer with an ISR 2200 integrating sphere attachment was used to determine the optical properties of titania powders and their suspensions. The diffuse reflectance spectra of all four powders utilized in the study were found to be almost identical. This strongly suggests the absence of quantum confinement effects frequently occurring in semiconductor nanoparticles. To determine the absorption and extinction coefficients, aqueous slurries of the powders of several different concentrations (0.025–0.25 g/L) were pre-ultrasonicated for 1 min at pH 4. They were placed into 1-cm quartz cuvettes for absorbance measurements at 355 nm. The absorbance was then plotted versus catalyst concentration, and the slopes yielded the corresponding optical characteristics. The measurement with an integrating sphere attachment gave the absorption coefficient (μ), and the measurement without the latter yielded the extinction coefficient (β). The scattering albedo (ω) was determined as a fraction of the light scattered away, $\omega = (\beta - \mu)/\beta$.

RESULTS AND DISCUSSION

At the beginning of this section we identify the dominating pathways for the reaction scheme [2.1]–[2.6]. In order to simplify the above reaction scheme one can use the knowledge obtained from homogeneous photochemistry. First, it is known that peroxide radicals and hydrogen peroxide do not react with formic acid in homogeneous solution (12). Our experiments with an initial concentration of formic acid of 30 mM and that of hydrogen peroxide of 30 mM proved this fact since they yielded no discernible conversion after 1 h. Hence, we can narrow down the number of reactive oxygen species to hydroxyl radicals. Furthermore, peroxide radicals (reaction [2.4]) form hydrogen peroxide, which when irradiated by UV light may produce two hydroxyl radicals according to the following reaction:

$$H_2O_2 \xrightarrow{h\nu} 2\,{}^{\bullet}OH. \qquad [4.1]$$

There are conflicting reports in the literature on the values of the quantum yield for this reaction in homogeneous medium. Calverts and Pitts (15) showed, however, that the absorption by hydrogen peroxide in the near-UV range (320–400 nm) is negligible, and reaction [4.1] takes place primarily under the mid- and far-UV radiation.

Independent experiments utilizing a modified Fricke dosimeter (13) can be performed to quantify the concentration of reactive oxygen species in an irradiated slurry. The following chemical transformations take place:

$$Fe^{2+} + {}^{\bullet}OH \rightarrow Fe^{3+} + OH^- \qquad [4.2.1]$$

$$Cu^{2+} + HO_2^{\bullet} \rightarrow Cu^+ + H^+ + O_2 \qquad [4.2.2]$$

$$Fe^{3+} + Cu^+ \rightarrow Fe^{2+} + Cu^{2+} \qquad [4.2.3]$$

$$2Fe^{2+} + H_2O_2 \rightarrow 2Fe^{3+} + 2OH^-. \qquad [4.2.4]$$

One can observe that two types of reactive oxygen species (hydroxyls and peroxide) participate in the oxidation of Fe^{2+}, producing three Fe^{3+} ions. The overall reaction is independent of the oxygen concentration as oxygen is liberated by reaction [4.2.2]. Since one of the three Fe^{3+} ions produced is scavenged by Cu^+ ions (reaction [4.2.3]), we have two radicals producing two iron(III) ions. Therefore, the oxidation rate of iron ions represents a realistic measure of the reactive oxygen species in photocatalytic solutions. Considering the irreversible bimolecular reaction rate law for the reaction of ferrous ions with reactive oxygen species,

$$-\frac{d[Fe^{2+}]}{dt} = k_{Fe^{2+}}[Fe^{2+}][O^{\nabla}]. \qquad [4.3]$$

The above relation is analogous to Eq. [2.6], and rearranging it yields

$$[O^{\nabla}] = -\frac{1}{k_{Fe^{2+}}}\frac{d\ln[Fe^{2+}]}{dt}. \qquad [4.4]$$

Replacing differentials in Eq. [4.4] with finite differences, one can determine the instantaneous concentration of radicals on the basis of known concentrations of the iron(II) ion. The values of the bimolecular reaction rate constants for the Fricke dosimeter are available in the literature (we will use the value of 2.5×10^8 L/(mol min) reported in Ref. (16)). The input of homogeneous photochemical oxidation (photo-Fenton process) was assessed for the Fricke dosimetry reactions and it contributed to about 5–10% of the activity. This is due to the instability of the ferrous ion in solution under illumination. To minimize this effect and to enable the dosimeter to work in less acidic media, cupric salts are added to the solution. Transition metal ions can absorb UV radiation as well as titania. In order to test the alteration of the radiation field in the reactor due to the absorption by the constituents of the Fricke solution, its optical density was analyzed at the wavelength of 355 nm (peak radiation in our reactor). This was done before the reaction and after 10 min of reaction (Degussa P25, 0.25 g/L). The absorbances found were in the range from 0.078 to 0.101, respectively. This corresponds to an absorbance by 0.25 g/L slurry of Degussa P25 in the vicinity of 2. Therefore, the maximum alteration of the photon flux by the transition metal ions employed can reach about 5% of the input of the absorption by titania. Furthermore, the above species are present in the solution in ionic form and therefore do not contribute to light scattering. This leads to the conclusion that the radiation fields

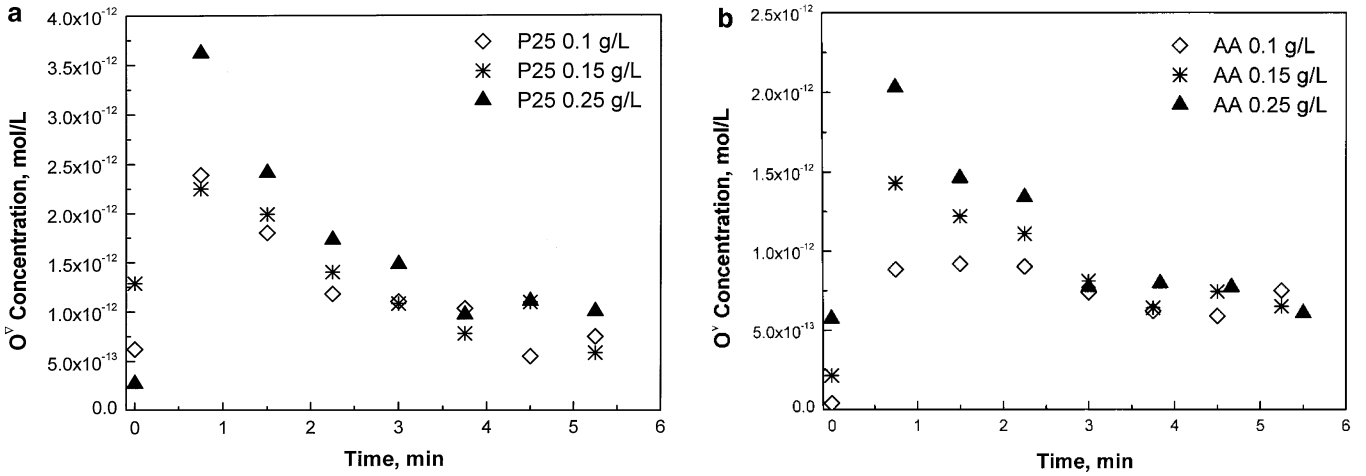

FIG. 1. Evolution of the concentration of reactive oxygen species in slurry (a) Degussa P25 (b) Aldrich anatase: $[Fe^{2+}]_0 = 0.03$ M, lamp power—450 W, temperature $30 \pm 3^{\circ}$C.

in the photodegradation of formic acid and oxidation of Fricke solution can be considered identical.The time dependence of the hydroxyl radical concentrations (calculated by using Eq. [4.4]) for two photocatalysts is shown in Figs. 1a (P25) and 1b (AA). One can observe that the steady-state concentration of these radicals is not achieved instantaneously. On the contrary, it passes through a maximum for all concentrations of AA and P25; the maximum becomes less pronounced at lower concentrations of the catalyst. This effect is due to the lower incipient surface area in the reactor and consequently a lower number of surface hydroxyls capable of becoming hydroxyl radicals. One can also observe that the maximum is less pronounced for AA. This is due to its lower BET surface area and the lower number of active sites of the latter catalyst. A similar trend (maximum of the concentration of primary radicals) was qualitatively predicted by Riegel and Bolton (17) and attributed to the lower rate of electron entrapment in comparison with that of hole entrapment. Thus, the trapped holes form more radicals at the beginning of the reaction than electrons do, until the recombination makes up for the excess of radical formation. Furthermore, these steady-state concentrations of primary radicals are in the order of 10^{-12} mol/L after several minutes of reaction. The total number of active sites (capable of becoming active radicals) of titania was estimated as 5×10^{18} m^{-2} by Pruden and Ollis (18). This corresponds to a "concentration" of active sites equal to 1.55×10^{-4} mol/L when a 0.25 g/L slurry of P25 is irradiated. One can observe that this value is considerably higher than that of the steady-state concentration of active radicals. Hence, a very small fraction of the catalytic sites of titania is actually active in the irradiated slurry. This fact is primarily due to inefficient light utilization and high electron–hole recombination rates (as will be shown later in this section).

In order to complete the above kinetic model, certain assumptions made in the theoretical section must be clarified experimentally. There has been extensive discussion in the literature (summarized in Ref. (19)) regarding whether organic molecules react with surface radicals of the excited semiconductor or with its holes directly during photodegradation. From general considerations, the latter is justifiable when the organic molecule and water can compete for the active sites of the photocatalyst or replace hydroxyl groups on its surface (3). This can be true for relatively high concentrations (order of moles per liter) of organics in the aqueous system (such as in the one reported in Ref. (11)). The vast majority of photocatalytic studies, however, deal with very low (order of ppm) concentrations. Additional evidence of the participation of primary radicals in the main oxidation reaction may be obtained by the photooxidation of inorganic ions, which cannot occur via radical mechanism. Indeed, a low photoreactivity of the illuminated ZnO electrode with respect to the oxidation of sulfite and bromide ions was observed (20). Herrmann and Pichat (21) found no photocatalytic activity to oxidize chloride ions by titania. To assess further the extent of direct oxidation by valence band holes, experiments were conducted utilizing oxygen as an electron scavenger and nitrite ion as a labile reducing agent, which followed the mechanism

$$NO_2^- + h^+ + H_2O \rightarrow NO_3^- + H^+ \qquad E = 0.934\,\text{V} \quad [4.5]$$

The extent of nitrite photodegradation can elucidate to which degree the UV-produced holes participate in the reaction directly. Experiments with initial sodium nitrite concentrations of 30 mM in a 0.25 g/L slurry of P25 showed very low rates of photooxidation. The latter were comparable with those of homogeneous oxidation by

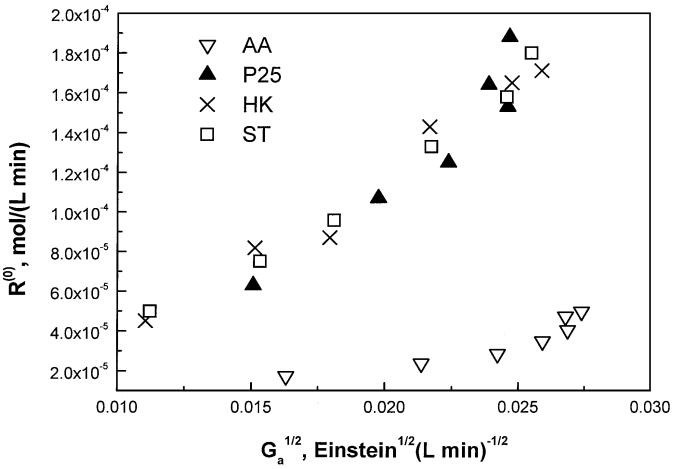

FIG. 2. Average zero-order rate of photodegradation of formic acid versus square root of the absorbed photon flux: $[HCOO^-]_0 = 30$ mM, lamp power—450 W, temperature $30 \pm 3°C$.

molecular oxygen in the dark with a total quantum yield in the order of 10^{-3} mol/Einstein, which is 2 orders of magnitude lower than that obtained with formic acid. This proves that the surface-reactive oxygen species are the main oxidizing agents in aqueous photocatalysis.

To obtain the lumped parameters of Eq. [3.5] of average zero-order, reaction rates can be plotted as a function of the volume-averaged square root of the absorbed photon flux in the reactor (Fig. 2). The absorbed photon flux was varied by changing the photocatalyst concentration in the slurry. One can measure experimentally the radiant flux on the cooling jacket using a radiation detector, thus obtaining a realistic profile of radiation entering the reaction zone. However, one needs to utilize modeling in order to determine the value of photon fluxes at different locations in the reactor (parameter G in Eq. [3.5]). This equation can then be integrated for each specific case and its constants can be determined. It was shown previously (14) that the shape of the axial radiation profile emitted by our mercury lamps remains almost unchanged after the radiation has passed through the reaction annulus. This leads to the conclusion that angular scattering can be neglected as the scattered beams compensate each other. The Schuster–Schwartzichild radiant-transfer approximation was developed for this case (22), and it will be applied to our system to determine radiant fluxes at any location in the reactor. This two-flux model assumes that the scattering remains isotropic throughout the vessel and the absorption and scattering of radiation are accounted for by two independent coefficients. Moreover, this model lumps together all forward-scattered beams into one flux and backward-scattered beams into another. We will therefore adopt the equation derived in Ref. (22) for the two-flux radiation transfer in a suspension of microorganisms with a modification for annular geometry. According to the model, the photon balance at each axial coordinate in the reactor space is given by

$$\frac{d(r\mathrm{F}^+)}{dr} = -C_{\mathrm{cat}}\mu r\mathrm{F}^+ + 1/2C_{\mathrm{cat}}\sigma(r\mathrm{F}^- - r\mathrm{F}^+) \quad [4.6.1]$$

$$\frac{d(r\mathrm{F}^-)}{dr} = C_{\mathrm{cat}}\mu r\mathrm{F}^- + 1/2C_{\mathrm{cat}}\sigma(r\mathrm{F}^- - r\mathrm{F}^+), \quad [4.6.2]$$

where F^+ corresponds to the forward photon flux, and F^- corresponds to the backward photon flux. Equations [4.6.1] and [4.6.2] are subject to the following boundary conditions:

$$r = R_{\mathrm{I}} : \mathrm{F}^+ = G_{\mathrm{I}}(z) \quad [4.6.3]$$

$$r = R_{\mathrm{O}} : \mathrm{F}^- = 0. \quad [4.6.4]$$

The solution of Eq. [4.6.1] and [4.6.2] for $G = \mathrm{F}^+ + \mathrm{F}^-$ with the boundary conditions [4.6.3] and [4.6.4] yields the following relation:

$$G(\bar{r},\bar{z}) = 2G_{\mathrm{I}}(\bar{z})\frac{R_{\mathrm{I}}}{\bar{r}(R_{\mathrm{O}}-R_{\mathrm{I}})+R_{\mathrm{I}}} \times \frac{(1+\alpha)\exp[-\delta(\bar{r}-1)] - (1-\alpha)\exp[\delta(\bar{r}-1)]}{(1+\alpha)^2\exp(\delta) - (1-\alpha)^2\exp(-\delta)}, \quad [4.6.5]$$

where G_{I} denotes the incident radiation (or radiant flux at the inner radius of the inner wall R_{I}, determined experimentally). The values of parameters α, δ, z, and r are determined from the following relations:

$$\bar{r} = \frac{r - R_{\mathrm{I}}}{R_{\mathrm{O}} - R_{\mathrm{I}}}$$
$$\bar{z} = \frac{z}{L}$$
$$\alpha = (1-\omega)^{1/2} \quad [4.6.6]$$
$$\delta = \beta C_{\mathrm{cat}}\alpha(R_{\mathrm{O}} - R_{\mathrm{I}}),$$

where R_{O} is the radius of the outer wall, r is the radial coordinate, $\omega = \sigma/\beta$ is scattering albedo, β is the extinction coefficient of the slurry, and C_{cat} is the photocatalyst concentration. In order to use Eq. [4.6.5] one needs to estimate the values of β and ω from independent spectrophotometric experiments without and with an integrating sphere, respectively. The values of the optical properties of the suspensions used are summarized in Table 1.

One can observe from Fig. 2 that for all four catalysts the linearity holds, which was also found by others (17). A slight reproducible deviation from linearity can be seen for AA at lower (0.05–0.15 g/L) concentrations. As reported before (4), the square-root dependence of the reaction rate (or quantum yield) on the absorbed photon flux may not hold for the entire range of fluxes. More specifically, at lower absorbed intensities this dependence becomes linear, thus

TABLE 2

Comparison of the Parameters of Eq. [3.5]

Catalyst	$k_{h^+}k_{e^-}/k_{rec}$, mol/(L min)	μ, L/(cm g)	k_s/k_{ct}, L/(mol min)[a]
AA	1.82×10^{-6}	9.38	40815
P25	3.25×10^{-5}	7.92	9756
HK	1.95×10^{-5}	9.39	1443
ST	2.00×10^{-5}	4.09	2477

[a] Determined at a catalyst concentration of 0.25 g/L, lamp power = 450 W, $[HCOO^-]_0 = 1.5$ mM, temperature $= 30 \pm 3°C$.

switching the kinetic regime with respect to the "concentration" of absorbed photons. Furthermore, the passage of the lines through the origin at zero absorbed photon flux should not be expected since at lower values of radiant flux the kinetic regime is different (Eq. [3.5]). Taking the slopes of these dependencies allow one to calculate the lumped kinetic parameter ($k_{h^+}k_{e^-}/k_{rec}$) for each photocatalyst. The values of this parameter determined with a degree of accuracy of 18% for AA and within 10% for the other three catalysts are presented in Table 2. The numerator of this parameter represents the cumulative rate of formation of active oxygen species and its denominator corresponds to the rate of electron–hole recombination. The values of this parameter are much lower than unity, which substantiates the widely accepted notion of electron-hole recombination rate as the pivotal determinant of photocatalyst efficiency (1). One can also observe that this ratio increases in the following fashion: AA < ST ≈ HK < P25. This behavior of Degussa P25 is justified by the presence of a rutile shell on each particle (17). It should be noted that rutile alone cannot act as an oxidation photocatalyst because of a different conduction band position and a considerably lower electron mobility in comparison with those of anatase. Furthermore, a refractory oxide coating (such as rutile) enhances charge separation, which in turn leads to lower recombination rates (23). The above lumped parameter is not proportional to the BET surface area of the photocatalyst. One would expect it to be proportional to BET area squared, since the rates of radical formation are surface rates and recombination occurs primarily in the bulk of the semiconductor. This behavior takes place because the entire surface of the high-BET area catalysts is not fully subjected to light in photoreactors. Indeed, the lifespan of a single particle of 5 nm size (HK-100) in a slurry is extremely small, after which it forms an aggregate with another particle, thus reducing the incipient surface of the catalyst.

As mentioned in the experimental section, experiments were performed with all the photocatalysts at relatively low concentrations of formic acid (starting with ~1.5 mM). The rate equation proved to be of shifting order. Indeed, the first multiplier of Eq. [3.5] is of Langmuir type; the reactant concentration–time dependence is illustrated in Fig. 3.

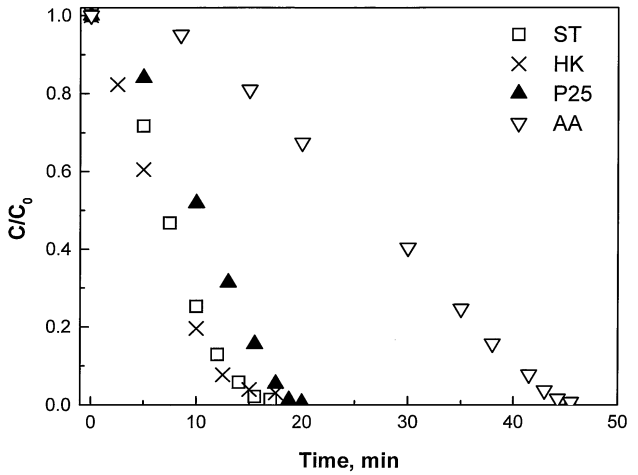

FIG. 3. Time course of the concentration of formic acid: $[HCOO^-]_0 = 1.5$ mM, lamp power—450 W, temperature $30 \pm 3°C$, catalyst concentration—0.25 g/L.

Similar trends were observed by Matthews (5), who also reported a low agreement between the experimental values at low conversions and those calculated by the Langmuirian model. This major discrepancy had the form of a "time lag" during the first few minutes. Moreover, since we observed a steady state of hydroxyl radicals after only 5 min on stream, we can integrate the time variable in Eq. [3.5] from some parameter t_d ("dead" time) instead of zero. Therefore, the integral Langmuir-type model becomes

$$t = k_1 \frac{[HCOO^-]}{[HCOO^-]_0} + k_2 \ln \frac{[HCOO^-]}{[HCOO^-]_0} + t_d, \qquad [4.7]$$

where $k_1 = -[HCOO^-]_0/R^{(0)}$ and $k_2 = -1/(R^{(0)}k_s/k_{ct})$. Furthermore, the parameter k_s/k_{ct} was extracted from Eq. [4.5] using curve-fitting software. The values of this parameter are shown in Fig. 4 as a function of catalyst concentration.

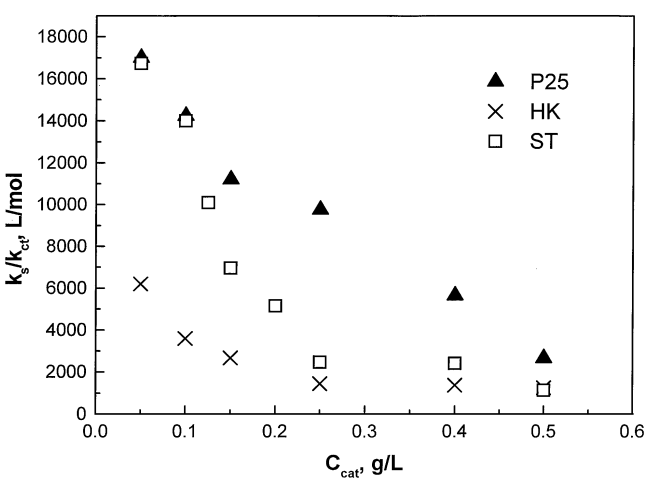

FIG. 4. Langmuir parameter of equation 3.5 versus catalyst concentration: $[HCOO^-]_0 = 1.5$ mM, lamp power—450 W, temperature $30 \pm 3°C$.

One can observe that this variable decreases monotonically with the increase in the photocatalyst loading for a wide range of concentrations (0.05–0.5 g/l). It should be noted that for AA the reactant concentration range corresponding to the first-order rate law is much shorter than those for the other three catalysts (Fig. 3), which did not allow us to elucidate a distinct trend of k_s/k_{ct} for AA. Its value for all catalysts is much higher than unity, which shows that the majority of the reactive oxygen species formed on the surface of the catalyst engage into the chemical reaction even at low concentrations of the reactant. As the catalyst concentration increases, so does the extent of recombination due to the lower concentration of the available reactant per gram of catalyst. For this reason the monotonic decrease of k_s/k_{ct} should be expected.

The comparison of the parameter k_s/k_{ct} for the catalysts employed in the study (Table 2) shows that the extent of reaction with the ambient organic are lower for the higher BET surface area catalysts (HK < ST < P25 < AA) for the catalyst concentration range tested in the present study. Therefore, the radicals formed on the surface of AA are much less likely to transfer their electron back to the solid particle in comparison with the engagement into chemical reactions with the ambient medium. This is because the sites of Aldrich anatase were found to be considerably more active than those of, for example, P25 (14).

Figures 5 and 6 show the rate of generation of active oxygen radicals (Eq. [3.8]) and electron–hole recombination (Eq. [3.9]) as a function of photocatalyst concentration for the four powders involved in the present study. The rate of radical generation represents the oxidative power of a particular catalyst. One can observe that it is the lowest for Aldrich anatase, however, not proportional to the BET surface area of catalysts (Table 1). It also attains a plateau

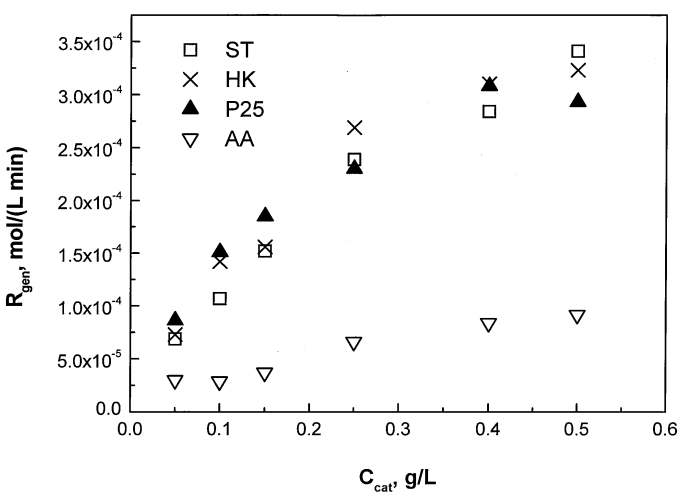

FIG. 5. Reactive oxygen species generation rates (Eq. [3.8]) as a function of photocatalyst concentration: lamp power—450 W, temperature $30 \pm 3°C$.

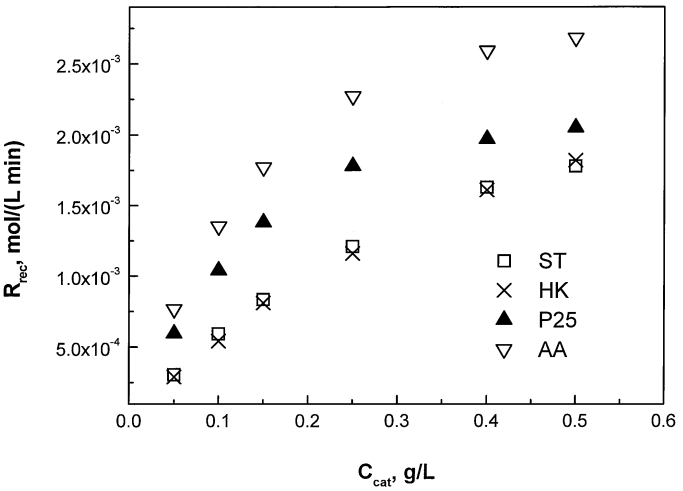

FIG. 6. Electron-hole recombination rates (Eq. [3.9]) versus photocatalyst concentration: lamp power—450 W, temperature $30 \pm 3°C$.

value at higher concentrations of photocatalyst as almost the entire portion of the photon flux becomes utilized in the reactor. One should also expect the lowering of this value at even higher concentrations of the photocatalyst since the smaller fraction of the reactor volume is subject to light. Furthermore, for the highest BET surface area catalyst (HK) the generation rate (Eq. [3.8]) is approximately the same as those for P25 and ST. This again underlines the fact that the working surface area of photocatalysts is much smaller than their total surface area, even for nonporous particles. The values of the generation rate (order of 10^{-4} mol/(L min)) divided by the photon absorption (order of 10^{-2} Einstein/(L min)) lead to quantum yields on the order of 10^{-2} mol/Einstein commonly encountered in heterogeneous photocatalysis. Therefore, in the absence of secondary radical oxidation reactions this is the limiting value for the quantum yield.

Figure 6 shows the rate of electron–hole recombination as a function of the photocatalyst concentration. It can be readily seen from this figure that the four photocatalysts behave similarly. A monotonic increase in the recombination rate is observed for all four catalysts with increasing concentration; it arrives at a plateau value for concentrations of 0.25 g/l and higher. Furthermore, the average electron–hole recombination for all catalysts with different physical properties (Table 1) is on the order of 10^{-3}. Such proximity of recombination rates is corroborated by the fact that the process of electron–hole recombination occurs in the bulk of the semiconductor. Therefore, since the core of each semiconductor photocatalyst utilized in this study is represented by anatase, the recombination rates are expected to be close. The highest recombination rates are observed for AA in the whole range of concentrations. This is because the particle size (Table 1) of the latter catalyst is much larger than those of all the others. This prompts a much higher hole

TABLE 3

Quantum Yields of Radical Generation and Electron–Hole Recombination

Catalyst	Quantum yield, mol/Einstein	
	Generation	Recombination
AA	0.0285 ± 0.007	0.972 ± 0.007
P25	0.122 ± 0.011	0.878 ± 0.011
HK	0.185 ± 0.029	0.816 ± 0.029
ST	0.172 ± 0.021	0.828 ± 0.021

diffusion length and, as a consequence, a higher probability of bulk recombination. By comparing Figs. 5 and 6 one can observe that the electron–hole recombination rate is considerably higher than that of generation of reactive oxygen species. This explains why quantum yields of photocatalytic degradation of organic compounds are lower than unity.

In order to compare the efficiency of each catalyst employed in the study for photochemical conversion of light one can also obtain quantum yields for primary processes such as those of radical generation and electron–hole recombination. These quantum yields are presented in Table 3 and they are independent of the catalyst concentration. One can observe that a 6–7-fold increase in the BET surface area (AA vs P25 and ST, Table 1) leads to a similar increase in the quantum yield of generation. However, further increase of the surface area (up to 313.2 for HK) leads to only ~5% enhancement. This apparently implies that the limit for our system (lamp, reactor, semiconductor species) has been achieved. Thus, the quantum yield of radical generation is an inherent characteristic of the oxidative powder of photocatalysts, and it is the highest number one could achieve in the absence recombination of radicals (reaction [2.5]) and secondary oxidation reactions. Furthermore, for all photocatalysts the quantum yield of electron–hole recombination is substantially larger than that of radical generation, again underlining the limitations of photocatalytic degradation in terms of energy efficiency, as the energy from recombination is largely lost.

In our earlier work we found that the apparent quantum yield of phenol and 2,4,6-trichlorophenol photodegradation can vary quite substantially (up to 6-fold) with the reactor setup [14]. To illustrate the applicability of the present method one can determine the quantum yields of the degradation of formic acid in two different photoreactors. The reactors tested corresponded to the conventional one (reaction zone size 24 cm × 0.6 cm, total volume 0.65 L) and the differential one (reaction zone size 12 cm × 0.15 cm, total volume 0.25 L). The quantum yields obtained for the four photocatalysts utilized in the present study at various concentrations (0.05–0.5 g/L) are presented in Table 4. The maximal difference in the quantum yields obtained from these two reactors is in the vicinity of 20% (for HK). Such a low difference is primarily due to the absence of secondary oxidation reactions taking place in the degradation of phenols. Heit and Braun (24) studied photolysis in aqueous systems and isolated two reactor volumes. These volumes correspond to a strongly irradiated primary reaction zone and a weakly illuminated secondary reaction zone, which occupies the major part of the reactor volume. The latter zone is dominated by the oxidation reactions between the organic and dissolved oxygen, hydrogen peroxide, and relatively stable oxygen radicals (such as peroxyl). Furthermore, in the case when single-stage complete oxidation of the reactant takes place, the secondary reaction volume does not exist. This is the primary reason for the small variability in the quantum yields of Table 4, and it justifies the validity of the proposed methodology. Furthermore, this fact substantiates our assumption of "high" photon flux in the reactor, which allowed us to neglect the unity under the square root in Eq. [3.5]. More specifically, one cannot expect the shift of the kinetic regime with respect to photons absorbed in a thin annulus, as the radial attenuation of light is low.

The turnover frequencies for each catalyst have also been calculated on the basic of the number of sites calculated by Pruden and Ollis (18). It was assumed that only the anatase phase of the titania powders possesses active sites. The much higher turnover number for AA is notable, although its apparent activity is the lowest. HK possesses the lowest turnover frequency because the degree of utilization of its surface is very low. Conclusively, the utilization of a single-stage oxidation reaction aids quantification of primary processes in heterogeneous photocatalysis and provides an elegant means of comparing different semiconducting powders.

TABLE 4

Quantum Yields of Formic Acid Degradation

Catalyst	Quantum yield, mol/Einstein		Turnover frequencies, s^{-1}
	Conventional	Differential	
AA	0.017 ± 0.002	0.018 ± 0.004	0.035
P25	0.082 ± 0.008	0.090 ± 0.008	0.022
HK	0.101 ± 0.018	0.081 ± 0.008	0.0037
ST	0.100 ± 0.019	0.094 ± 0.002	0.018

CONCLUSIONS

The quantification of primary photocatalytic processes was performed for selected titania powders by utilizing a single-stage oxidation reaction, namely, the photodegradation of HCOOH. It elucidated the effect of BET surface area and phase composition of the photocatalysts on their behavior. In particular, the concentration of reactive oxygen species was found to pass through a maximum and attain a steady state. Furthermore, the rate of

generation of these species increases monotonically with catalyst concentration and arrives at a plateau value in the concentration vicinity of 0.25 g/l. This generation rate follows the pattern ST ≈ HK ≈ P25 > AA; its value for Aldrich anatase is approximately one-third that for the other catalysts. In contrast, the electron–hole recombination rate was the highest for the latter catalyst and changed in the following order: AA > P25 > ST ≈ HK. The highest value for Aldrich anatase is related to its large primary particle size, which leads to a higher diffusion length for the charges to reach the surface of the particle. Furthermore, the knowledge of primary rates of photocatalysis reveals the nature of low quantum yields commonly encountered and can provide an objective means to compare different photocatalysts.

NOMENCLATURE

C_{cat} photocatalyst concentration, g/l
F^+ forward photon flux density, Einstein/(cm^2 min)
F^- backward photon flux density, Einstein/(cm^2 min)
G photon flux density, Einstein/(cm^2 min)
G_a absorbed photon flux density, Einstein/(L min)
G_I density of the photon flux entering reaction zone, Einstein/(cm^2 min)
k_1 constant of Eq. [4.7]
k_2 constant of Eq. [4.7]
k_{ct} radical recombination (charge-transfer) reaction [2.5] rate constant, 1/min
k_{e^-} surface electron reaction rate constant, 1/min
$k_{Fe^{2+}}$ bimolecular surface reaction rate constant of Fe^{2+} ion oxidation, L/(mol min)
k_{h^+} surface hole reaction rate constant, 1/min
k_{rec} electron–hole recombination rate constant, L/(mol min)
k_s bimolecular surface reaction [2.6] rate constant, L/(mol min)
L reactor length, cm
r reactor radius, cm
$R^{(0)}$ reaction rate of photodegradation (zero order), mol/(L min)
$R^{(1)}$ reaction rate of photodegradation (first order), mol/(L min)
R_{ct} charge-transfer reaction [5] rate, mol/(L min)
R_{e^-} surface electron reaction rate, mol/(L min)
R_{ex} excitation rate, mol/(L min)
R_{gen} radical generation rate, mol/(L min)
R_{h^+} surface hole reaction rate, mol/(L min)
R_n reaction rate of the nth process, mol/(L min)
R_{rec} electron–hole recombination rate, mol/(L min)
R_s bimolecular surface reaction [6] rate, mol/(L min)
R_I inner radius of the reaction zone, cm
R_O outer radius of the reaction zone, cm
t time, min
t_d dead time, min
z axial coordinate, cm

Greek Symbols

α parameter of Eq. [4.6.2]
β extinction coefficient of the photocatalyst slurry, L/(g cm)
δ parameter of Eq. [4.6.2]
μ absorption coefficient of the photocatalyst slurry, L/(g cm)
σ scattering coefficient of the photocatalyst slurry, L/(g cm)
ω scattering albedo of the photocatalyst slurry
Φ quantum yield, mol/Einstein

ACKNOWLEDGMENTS

The authors acknowledge the Technical Association of Pulp and Paper Industry (TAPPI) for supporting this work through Grant No. PE-380-97.

REFERENCES

1. Hoffmann, M. R., Martin, S. T., Choi, W., and Bahnemann, D. W., *Chem. Rev.* **95**, 69 (1995).
2. Turchi, C. S., and Ollis, D. F., *J. Catal.* **122**, 178 (1990).
3. Sun, L., and Bolton, J. R., *J. Phys. Chem.* **100**, 4127 (1996).
4. Schwarz, P. F., Turro, N. J., Bossmann, S. H., Braun, A. M., Wahab, A.-M., and Dürr, H., *J. Phys. Chem. B* **101**, 7127 (1997).
5. Matthews, R. W., *Water Res.* **24**, 653 (1990).
6. Morrison, S. R., and Freund, T., *J. Chem. Phys.* **47**, 1543 (1967).
7. Micka, K., and Gerischer, H., *J. Electroanal. Chem.* **38**, 397 (1972).
8. Matsumura, M., Hiramoto, M., Iehara, T., and Tsubomura, H., *J. Phys. Chem.* **88**, 248 (1984).
9. Aguado, M. A., Anderson, M. A., and Hill, C. G., *J. Mol. Catal.* **89**, 165 (1994).
10. Ha, H. Y., and Anderson, M. A., *J. Environ. Eng.* 217 (1996).
11. Benderskii, V. A., Zolotovskii, Ya. M., Kogan, Ya. L., Khidekel', M. L., and Shub, D. M., *Dokl. Akad. Nauk SSSR* **222**, 606 (1975).
12. Draganić, I. G., and Draganić, Z. D., "Radiation Chemistry of Water," Academic Press, San Diego, 1971.
13. Fricke, H., and Hart, E. J., "Radiation Dosimetry," Vol. II, p. 167 Academic Press, San Diego, 1966.
14. Davydov, L., Smirniotis, P. G., and Pratsinis, S. E., *Ind. Eng. Chem. Res.* **38**, 1376 (1999).
15. Calverts, J. G., and Pitts, J. N., "Photochemistry," Wiley, New york, 1967.
16. Anbar, M., and Neta, P., *Int. J. Appl. Radiat. Iso.* **18**, 493 (1967).
17. Riegel, G., and Bolton, J. R., *J. Phys. Chem.* **99**, 4215 (1995).
18. Pruden, A. L., and Ollis, D. F., *J. Catal.* **82**, 404 (1983).
19. Pelizzetti, E., *Sol. Energ. Mater. Sol. Cells* **38**, 453 (1995).
20. Gomes, W. P., Freund, T., and Morrison, S. R., *J. Electrochem. Soc.* **115**, 818 (1968).
21. Herrmann, J.-M., and Pichat, P., *J. Chem. Soc., Faraday Trans. 1* **76**, 1138 (1980).
22. Cornet, J. F., Dussap, C. G., and Dubertret, G., *Biotech. Bioeng.* **40**, 817 (1992).
23. Kamat, P. V., *Chem. Rev.* **93**, 267 (1993).
24. Heit, G., and Braun, A. M., *Water Sci. Technol.* **35**, 25 (1997).